How fast is a twisted photon?

Research Article Vol. 5, No. 6 / June 2018 / Optica 682

How fast is a twisted photon?

Ashley Lyons,[1,2] Thomas Roger,[1] Niclas Westerberg,[1] Stefano Vezzoli,[1] Calum Maitland,[1] Jonathan Leach,[1] Miles J. Padgett,[2] and Daniele Faccio[1,2,*]

[1]School of Engineering and Physical Sciences, Heriot-Watt University, Edinburgh EH14 4AS, UK
[2]School of Physics and Astronomy, University of Glasgow, Glasgow G12 8QQ, UK
*Corresponding author: daniele.faccio@glasgow.ac.uk

Received 2 March 2018; revised 20 April 2018; accepted 23 April 2018 (Doc. ID 325089); published 25 May 2018

Recent measurements have highlighted that even in vacuum spatially shaped photons travel slower than *c*, the speed of monochromatic plane waves. Here we investigate the *intrinsic* delay introduced by "twisting" a photon, i.e., by introducing orbital angular momentum (OAM), and measure the photon time of flight with a Hong–Ou–Mandel interferometer. When all other parameters are held constant, the addition of OAM reduces the delay (accelerates) with respect to the same beam with no OAM. We support our results using a theoretical method to calculate the group velocity and gain an intuitive understanding of the measured OAM acceleration by considering a geometrical ray-tracing approach.

OCIS codes: (270.0270) Quantum optics; (120.3180) Interferometry.
https://doi.org/10.1364/OPTICA.5.000682

1. INTRODUCTION

The propagation velocity of light in vacuum is a constant, c, only for monochromatic plane waves: any deviation from the plane-wave constraint can lead to a propagation velocity different from c. Even the simplest of light beams, such as a focused Gaussian beam, exhibits regions of modified group velocity [1]. A whole range of more complicated beams that are appropriately shaped in space, time, or space and time have been identified, which exhibit intensity peaks and structures that are subluminal, superluminal, or accelerating [2–9].

A slightly more fundamental issue has been addressed recently, namely, the propagation time of a single photon from one point (the "source") to another (the "detector"), thus highlighting that the beam structure will modify the propagation time [10]. The group velocity of a photon structured in the transverse dimension propagating in vacuum can be calculated as

$$\langle v_g^{(z)} \rangle = \left\langle \left(\frac{\partial^2 \phi(\boldsymbol{r})}{\partial_\omega \partial_z} \right)_{\omega_0} \right\rangle^{-1}, \tag{1}$$

where ∂_ω and ∂_z indicate, respectively, the gradient with respect to the photon carrier frequency ω and the position along the propagation direction z, and $\phi(\boldsymbol{r})$ represents the phase front in the cylindrical coordinates $\boldsymbol{r} = (r, \varphi, z)$ [10–12]. Here $\langle \ldots \rangle$ denotes the spatial average over the transverse beam structure, using the normalized field intensity as a weight. In the case of a plane wave, $\partial_z \phi(\boldsymbol{r}) = k_0$, where $k_0 = 2\pi/\lambda$ is the vacuum wavevector of the photon with a wavelength of λ. This plane wave provides the standard result that in vacuum the group velocity is equal to the speed of light $c = \omega/k_0$. However, as soon as there is a spatial structure of any kind on the transverse photon profile, $\partial_z \phi(\boldsymbol{r})$ is a non-trivial function of ω such that the speed along the propagation direction will deviate from c. An intuitive understanding of this deviation is based on the simple observation that c is the speed of a monochromatic plane wave (as can be seen upon inspection of the Maxwell equations), and that in a structured photon, the constituent plane waves are propagating at non-zero angles with respect to the propagation axis. The travel time of a photon from one point "A" to another point "B" is longer due to these plane-wave components traveling at an angle with respect to the axis connecting A to B (and, hence, travel a longer distance). It is, therefore, intuitively clear that the propagation time of a focused (e.g., imaged from the source to the detector) photon will increase as the ring radius is increased. This delay as a function of radius is also well described within the framework of a simple ray-tracing theory [10].

The propagation of light with an azimuthal phase gradient, i.e., orbital angular momentum (OAM), was also examined recently [12,13]. In this case, one must allow for the fact that these beams have a ring-shaped spatial profile and that for increasing OAM, the ring radius also naturally increases for the typical beam types encountered in experiments, e.g., Laguerre–Gauss (LG) or hypergeometric beams. The introduction of OAM will therefore lead to the observation of a delay for increasing OAM due the increasing ring size [12].

Here we address the fundamental question of the intrinsic effect of OAM on the propagation time of a single photon. This requires separating the effect of increasing OAM from the effect of the associated increase in ring radius in naturally

occurring OAM modes. Our measurements show that, rather counterintuitively, OAM *increases* the velocity of the photon when compared with a photon that has exactly the same spatial profile but is carrying zero OAM. These findings are supported by a theoretical model and ray-tracing considerations providing intuitive explanations for the observed effect. Although the two-photon interference, which necessitates the use of single photons, is used to demonstrate the phenomenon here, this effect is equivalently present in classical beams possessing OAM.

The effective change in velocity of beams carrying OAM may have consequences in a number of quantum technologies, such as quantum key distribution [14,15], which use OAM due to its inherent high dimensionality [16–18]. For example, accurate timing of signals used in quantum communications may be affected if the velocity of the photons is calculated incorrectly [19]. Furthermore, measurements of photons in cosmology could be subject to discrepancies in arrival time if these subtle effects are not properly accounted for [20].

2. EXPERIMENTS

We wish to study the propagation velocity of photons with a fixed spatial profile, specifically, with a ring-shaped intensity distribution. Careful control of the transverse shape of the photons can be achieved with an spatial light modulator (SLM), which can also be used to impart the required OAM. In our experiment, indistinguishable photon pairs are generated via spontaneous parametric down-conversion in a nonlinear crystal pumped by 100 fs, 404 nm wavelength pulses, provided by a frequency-doubled 80 MHz, Ti:sapphire oscillator. The experimental arrangement is thereafter the same as that described in Ref. [10] (see Fig. 1 for details). The two photons are separated; one photon is used as a reference, whereas the other is sent via a pair of SLMs. The first SLM imprints the desired phase structure, whereas the second applies the inverse phase to return the photon to a plane-wave mode. In all the experiments (aside from the plane-wave reference), a focusing lens phase is imprinted on each of the SLMs to form a $4f$ telescope between the input and output fibers. The signal and reference photons are recombined at a 50:50 fiber beam splitter where they undergo Hong–Ou–Mandel (HOM) interference [21] and produce the characteristic HOM dip as the variable path delay of the reference photon is scanned. The photons are detected via two single-photon avalanche detectors (Excelitas SPCM-14) and counted in coincidence via an event timing module (PicoQuant HydraHarp 400). The position of the HOM dip minimum is used to define the average transit time of the structured photons. For each delay position of the reference photon (controlled with a stepper motor) along the HOM dip, we iteratively imprint *all* of the various ring-shaped holograms ($m = 0$–8) onto the SLMs and integrate the coincidence counts for 2 s for each m. The full delay-scan measurement is then repeated 90 times and we take the final averaged (over the 90 independent measurements) HOM dip minimum and standard deviation error. This procedure (see Supplement 1 for more details) effectively minimizes systematic errors, for instance, due to thermal fluctuations, and allows increasing precision through averaging over random contributions to variations in the measured HOM dip position. To remove the radial dependence, we performed experiments with a ring-shaped mask applied to the beam, where we choose for each m the size of the mask to match the natural size of a LG beam after propagation to the far field, given by $D(m) = 2w\sqrt{|m|/2}$, where w is the beam waist. The phase ($2\pi m$ in the range $0 < m < 8$) and amplitude mask were imposed onto the beam using the first SLM along with a focusing lens phase with a focal length of $f = 300$ mm. We also measured, for reference, the HOM dip position for a Gaussian beam ($m = 0$), i.e., no structuring of the transverse phase. Any systematic delays (due to, for example, the SLMs) are removed by only considering the relative difference in optical delay between measurements with/without OAM and the same intensity profile. Figure 2 shows the data with OAM (red squares) and without OAM (blue circles). We observe that *all* of the measurements with OAM lie below those without OAM, thus clearly indicating that photons with OAM suffer less delay than the same (intensity profile) photons with no OAM. In order to assess the impact of the statistical relevance of the data (large error bars in Fig. 2), we provide an analysis to compare our data with the "null hypothesis," i.e., with the hypothesis that there is no difference in delay between the photons with OAM and the photons with no OAM. In Fig. 3(a), we show the difference between the photon delays, i.e., the difference between the two sets of data in Fig. 2, $\Delta[\delta z] = \delta z_{m>0} - \delta z_{m=0}$. Taking into account that there cannot be a difference for $m = 0$ and that the OAM effect should increase with m, we fit the data with the simplest phenomenological model, a straight line, weighted with the measurement errors. The darker shaded region shows the 1σ confidence bound of the fit to the data, whereas the lighter shaded area shows the 3σ confidence bound. As can be seen, the null hypothesis cannot explain the data with a confidence that is slightly better than 3σ.

Therefore, when considered together, the data show with 3σ confidence that OAM contributes to the group velocity of a photon and that this contribution leads to a speed up of the photon.

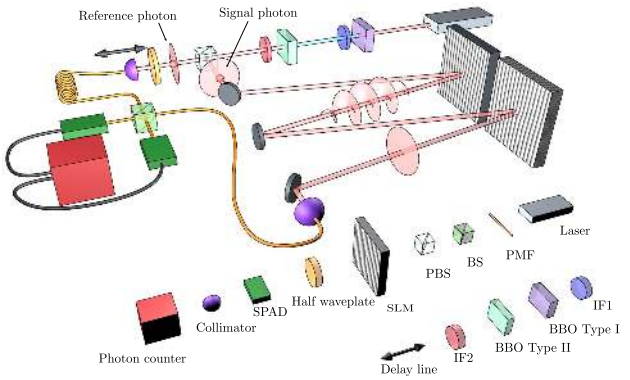

Fig. 1. Experimental setup to study the path length traveled by a structured photon. Pulses of light with a central wavelength of 404 nm are produced by frequency-doubling a Ti:sapphire laser in a type-I beta-barium borate (BBO) crystal. Photon pairs at 808 nm are generated in a type-II BBO crystal. The photons are polarized orthogonally and are split on a polarizing beam splitter. One photon is spatially structured via an SLM, whereas the other photon (reference) is coupled to a polarization-maintaining fiber (PMF) with the input end mounted on a stepper motor so as to finely control the length of free-space propagation before the fiber and, therefore, the optical delay (delay line). The phase structure of the structured photon is returned to a Gaussian beam by a second SLM and coupled into a PMF and recombined with the reference photon on a 50:50 beam splitter where the photons undergo HOM interference. Single-photon detectors are used to coincidence count the output photons. The position of the HOM interference dip measures the transit time of the signal photon.

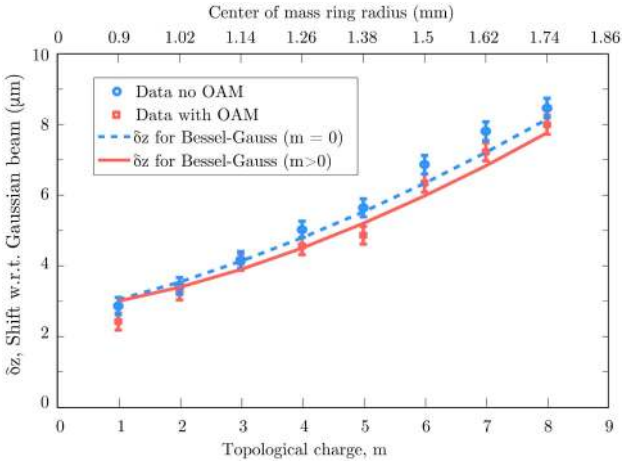

Fig. 2. Experimental results. Photon path delay, measured relative to a Gaussian ($m = 0$) beam, for photons with a ring aperture for the cases with (red squares) and without (blue circles) OAM. The ring diameter of the photons is $D(m) = 2w\sqrt{|m|/2}$. The lines show the theoretical predictions based on Eq. (5).

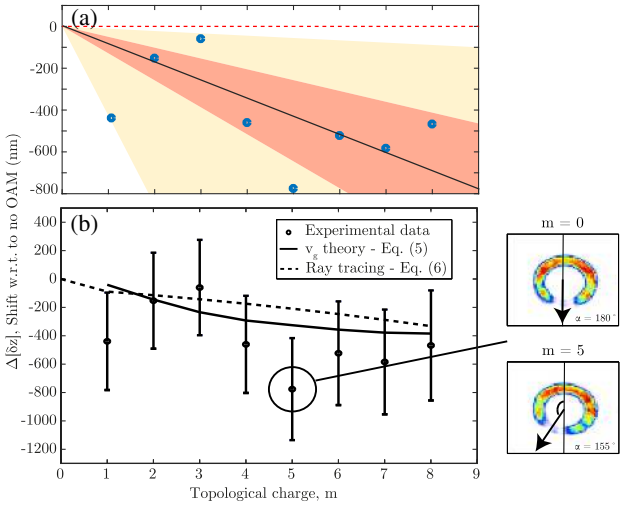

Fig. 3. Effect of adding OAM to beams with a ring aperture. (a) We show the difference in path length between ring-shaped photons with and without OAM, $\Delta[\delta z] = \delta z_{m>0} - \delta z_{m=0}$. The solid black line is the error-weighted, linear regression of the data. The dark (light) shaded area shows the $1\sigma(3\sigma)$ confidence bound. The null hypothesis ($\Delta[\delta z] = 0$) is shown as a dashed red line: this cannot explain the data with a confidence better than 3σ. (b) The data are fit using the full theoretical description of the group velocity for Bessel–Gauss modes Eq. (5) (solid line) and the ray-tracing approach using Eq. (6) (dashed line). The insets show transverse profiles of the $m = 0$, 5 intensity profiles measured using a continuous-wave source. A wedge is removed from the ring to illustrate that adding OAM rotates the intensity profile by an angle measured to be $\alpha = 155°$ for all values of m.

A simple theoretical model can provide a physical justification and insight into this surprising effect.

3. THEORY

One simple set of modes to consider is the Bessel–Gauss set [22]. These beams exhibit an extended depth of field and an annular intensity distribution in the far field [23–25]. Following Ref. [10], the z-averaged velocity of a photon can be expressed as

$$\overline{v_g} = \frac{L}{\int_{z_1}^{z_2} \mathrm{d}z \langle v_g^{(z)} \rangle^{-1}}, \tag{2}$$

where $L = z_2 - z_1$ and where z_1 and z_2 indicate, respectively, the start (source) and end (detector) positions of the photon path. The time taken for a photon to travel L is thus $t = L/\overline{v_g}$, and the distance between a structured photon and a plane wave that travels at constant speed of c over a fixed time is given by

$$\delta z = ct - L = \left[\frac{\partial}{\partial k}(\arg\langle\psi(\boldsymbol{r}, k_0)|\psi(\boldsymbol{r}, k)\rangle)|_{k_0} - z\right]_{z_1}^{z_2}, \tag{3}$$

where arg is the complex argument, and $|\psi(\boldsymbol{r}, k)\rangle$ is the normalized field amplitude such that $\langle\psi|\psi\rangle$ denotes the overlap integral in the transverse plane (r, ϕ). In the case of the paraxial wave approximation, this simplifies to [10]

$$\overline{v_g} = \frac{c}{1 + \frac{\langle \mathbf{k}_\perp^2 \rangle_{z_1}}{2k_0^2}} \approx c\left(1 - \frac{\langle \mathbf{k}_\perp^2 \rangle_{z_1}}{2k_0^2}\right) \tag{4}$$

and

$$\delta z = \frac{L}{2k_0^2}\langle \mathbf{k}_\perp^2 \rangle_{z_1}, \tag{5}$$

where $\langle \ldots \rangle_{z_1}$ denotes average over the normalized field amplitude at the source $z = z_1$ and $\mathbf{k}_\perp$ is the transverse wavevector.

This analysis provides a rigorous estimation of the change in the propagation velocity of the structured photons we use in the experiments. Numerical estimation of Eq. (5) gives the dashed and solid lines in Fig. 2.

An intuitive model of the influence of OAM on the speed of a photon may also be obtained within the context of a geometrical ray description [26]. The delay is estimated by considering the photon propagation from the plane of the "source" to that of the "detector," i.e., the object and image planes of a non-magnifying telescope. A Laguerre–Gauss $\mathrm{LG}_{0,0}$ mode (a Gaussian mode with no OAM) will be spatially inverted as it travels through the beam waist, i.e., images will appear inverted at the telescope imaging plane. In Fig. 4(a), we show the Poynting vector for this mode (indicated as "lens ray") that goes through an effective rotation of $\alpha = 180°$ in the transverse plane. A Laguerre–Gauss $\mathrm{LG}_{m,0}$ mode

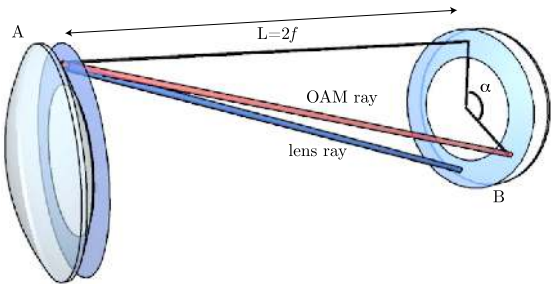

Fig. 4. Ray picture of the plane-wave trajectories in the case of a fixed-diameter ring-shaped beam passing through the focus of a telescope formed between lenses placed at positions A and B (separated by a distance of $L = 2f$). In the zero-OAM $m = 0$ case (indicated as "lens ray"), images are inverted, corresponding to a rotation of the ray by an angle of $\alpha = 180°$. Introducing OAM (indicated as "OAM ray") necessarily leads to a smaller rotation angle of α and thus to a shorter path length covered by the respective Gaussian beam, i.e., to an acceleration of the photon.

with an OAM integer m behaves somewhat differently: the Poynting vector no longer rotates by 180°. Rather, the vector rotates by an angle that is smaller in absolute value and in either a clockwise or a counter-clockwise direction depending on the sign of the OAM [27].

Using this geometrical insight, it is therefore possible to estimate the photon path difference between a generic ring-shaped beam with and without OAM (but with a fixed ring radius):

$$\delta z_{\mathrm{RayTracing}} = \left(\frac{1}{2} - \frac{1-\cos\alpha}{4}\right)\frac{D^2}{L}, \tag{6}$$

where L is the distance between the two lenses and D is the diameter of the intensity ring. As can be seen from the ray-tracing Eq. (6), any OAM will actually *advance* the photon arrival with respect to a beam with the same intensity profile and $m = 0$. In other words, the longest possible trajectory that a light ray can take is given by image inversion, $\alpha = 180°$, corresponding to what is expected for an $m = 0$ beam. If one adds OAM, the rays will then be skewed yet still remain rays, i.e., straight lines that can therefore only connect the object to the image plane via trajectories that are shortened. These shortened trajectories imply a faster transit time for photons that carry OAM with respect to photons that carry none.

The delay difference between OAM and no OAM is compared with the theory in Fig. 3(b). The solid line shows the prediction based on Eq. (5) for Bessel–Gauss modes similar to those used in the experiments. The curve uses the exact radial distribution measured in the experiments and thus has *no free* parameters. The dashed line shows the expected delays calculated from the simpler ray-tracing theory. This ray-tracing approach requires knowledge of the Poynting vector rotation angle α. We thus performed additional measurements with a standard diode laser injected into the arm containing the SLMs. We then impose the same phase and amplitude masks as for the single-photon experiments, but now with a 45° slice removed around $\alpha = 0°$. The insets in Fig. 3(b) show just one example: for $m = 0$, the "slice" is rotated by $\alpha = 180°$, corresponding to the expected image inversion for our telescopic imaging setup, whereas for $m = 5$ the slice is only rotated by $\alpha = \pm 155°$. We verified that this rotation is independent of the OAM winding number. We therefore use this value of α in Eq. (6).

Both models correctly predict the observed trend of the data, i.e., a negative delay shift of the photons with OAM whose absolute value is increasing with the topological number m. Due to the standard deviation error of the measurements, we can only affirm that both models agree within 1 standard deviation with the data. This agreement is nevertheless rather remarkable considering both models have no free parameters and thus support the conclusion that OAM speeds up a photon. Although both models discussed above were used to directly compare with the $4f$ telescope in our experimental setup, the effects described are general and apply to any beam carrying OAM that propagates in free space from the near field to the far-field (or focal plane of a lens.

4. CONCLUSIONS

We have shown experimentally that the introduction of OAM onto a photon reduces its transit time over a fixed path length. This result is not in contradiction with previous results where the spatial profile of a classical light beam was allowed to vary as OAM was introduced. The main purpose of our study here is that we are investigating the intrinsic OAM delay, rather than the overall effect due to both OAM and *spatial reshaping* of the beam due to the OAM. This acceleration of the photon due to OAM can be understood within the framework of ray optics and is related to the fact that the longest path for a ray is given by rays that invert an image through a telescope. Beams or photons with OAM rotate images by an angle that is always less than 180° and, hence, energy flows along shorter paths. We also show that a more rigorous description can be obtained by explicitly calculating the group velocity [see Eq. (1)]. We underline that the main result of this work is the experimental verification, with a confidence of 3σ, that the intrinsic effect of OAM is to speed up the photon.

Funding. Engineering and Physical Sciences Research Council (EPSRC) (EP/M006514/1, EP/M01326X/1, EP/L015110/1); H2020 European Research Council (ERC) (ERC GA 306559, ERC GA 340507).

Acknowledgment. D. F. acknowledges financial support from the EPSRC. M. J. P. and D. F. acknowledge financial support from the ERC. N. W. and C. M. acknowledge support from EPSRC.

See Supplement 1 for supporting content. All data related to this work can be obtained from DOI: https://10.17861/186d52be-1b78-46c5-9a55-fa4905e366ff.

REFERENCES

1. Z. L. Horváth, J. Vinkó, Z. Bor, and D. von der Linde, "Acceleration of femtosecond pulses to superluminal velocities by Gouy phase shift," Appl. Phys. B **63**, 481–484 (1996).
2. D. Mugnai, A. Ranfagni, and R. Ruggeri, "Observation of superluminal behaviors in wave propagation," Phys. Rev. Lett. **84**, 4830–4833 (2000).
3. I. Alexeev, K. Y. Kim, and H. M. Milchberg, "Measurement of the superluminal group velocity of an ultrashort Bessel beam pulse," Phys. Rev. Lett. **88**, 073901 (2002).
4. P. Bowlan, H. Valtna-Lukner, M. Lõhmus, P. Piksarv, P. Saari, and R. Trebino, "Measuring the spatiotemporal field of ultrashort Bessel-X pulses," Opt. Lett. **34**, 2276–2278 (2009).
5. H. Valtna-Lukner, P. Bowlan, M. Lõhmus, P. Piksarv, R. Trebino, and P. Saari, "Direct spatiotemporal measurements of accelerating ultrashort Bessel-type light bullets," Opt. Express **17**, 14948–14955 (2009).
6. F. Bonaretti, D. Faccio, M. Clerici, J. Biegert, and P. D. Trapani, "Spatiotemporal amplitude and phase retrieval of Bessel-X pulses using a Hartmann–Shack sensor," Opt. Express **17**, 9804–9809 (2009).
7. A. Chong, W. H. Renninger, D. N. Christodoulides, and F. W. Wise, "Airy Bessel wave packets as versatile linear light bullets," Nat. Photonics **4**, 103–106 (2010).
8. M. Lõhmus, P. Bowlan, P. Piksarv, H. Valtna-Lukner, R. Trebino, and P. Saari, "Diffraction of ultrashort optical pulses from circularly symmetric binary phase gratings," Opt. Lett. **37**, 1238–1240 (2012).
9. P. Piksarv, H. Valtna-Lukner, A. Valdmann, M. Lõhmus, R. Matt, and P. Saari, "Temporal focusing of ultrashort pulsed Bessel beams into Airy-Bessel light bullets," Opt. Express **20**, 17220–17229 (2012).
10. D. Giovannini, J. Romero, V. Potoček, G. Ferenczi, F. Speirits, S. M. Barnett, D. Faccio, and M. J. Padgett, "Spatially structured photons that travel in free space slower than the speed of light," Science **347**, 857–860 (2015).
11. M. Born, E. Wolf, and A. B. Bhatia, *Principles of Optics* (Cambridge University, 1999), Chap. 1, Eq. (56).
12. F. Bouchard, J. Harris, H. Mand, R. W. Boyd, and E. Karimi, "Observation of subluminal twisted light in vacuum," Optica **3**, 351–354 (2016).
13. N. D. Bareza and N. Hermosa, "Subluminal group velocity and dispersion of Laguerre–Gauss beams in free space," Sci. Rep. **6**, 26842 (2016).
14. M. Mafu, A. Dudley, S. Goyal, D. Giovannini, M. McLaren, M. J. Padgett, T. Konrad, F. Petruccione, N. Lütkenhaus, and A. Forbes,

"Higher-dimensional orbital-angular-momentum-based quantum key distribution with mutually unbiased bases," Phys. Rev. A **88**, 032305 (2013).
15. M. Mirhosseini, O. S. Magaña-Loaiza, M. N. O'Sullivan, B. Rodenburg, M. Malik, M. P. J. Lavery, M. J. Padgett, D. J. Gauthier, and R. W. Boyd, "High-dimensional quantum cryptography with twisted light," New J. Phys. **17**, 033033 (2015).
16. J. Leach, B. Jack, J. Romero, A. K. Jha, A. M. Yao, S. Franke-Arnold, D. G. Ireland, R. W. Boyd, S. M. Barnett, and M. J. Padgett, "Quantum correlations in optical angle-orbital angular momentum variables," Science **329**, 662–665 (2010).
17. M. Agnew, J. Leach, M. McLaren, F. S. Roux, and R. W. Boyd, "Tomography of the quantum state of photons entangled in high dimensions," Phys. Rev. A **84**, 62101 (2011).
18. A. C. Dada, J. Leach, G. S. Buller, M. J. Padgett, and E. Andersson, "Experimental high-dimensional two-photon entanglement and violations of generalized Bell inequalities," Nat. Phys. **7**, 677–680 (2011).
19. G. Gibson, J. Courtial, M. J. Padgett, M. Vasnetsov, V. Pas'ko, S. M. Barnett, and S. Franke-Arnold, "Free-space information transfer using light beams carrying orbital angular momentum," Opt. Express **12**, 5448–5456 (2004).
20. S. Chelkowski, S. Hild, and A. Freise, "Prospects of higher-order Laguerre–Gauss modes in future gravitational wave detectors," Phys. Rev. D **79**, 122002 (2009).
21. C. K. Hong, Z. Y. Ou, and L. Mandel, "Measurement of subpicosecond time intervals between two photons by interference," Phys. Rev. Lett. **59**, 2044–2046 (1987).
22. D. N. Schimpf, J. Schulte, W. P. Putnam, and F. X. Kärtner, "Generalizing higher-order Bessel–Gauss beams: analytical description and demonstration," Opt. Express **20**, 26852–26867 (2012).
23. V. Bagini, F. Frezza, M. Santarsiero, G. Schettini, and G. S. Spagnolo, "Generalized Bessel–Gauss beams," J. Mod. Opt. **43**, 1155–1166 (1996).
24. R. Vasilyeu, A. Dudley, N. Khilo, and A. Forbes, "Generating superpositions of higher-order Bessel beams," Opt. Express **17**, 23389–23395 (2009).
25. J. C. Gutiérrez-Vega and M. A. Bandres, "Helmholtz–Gauss waves," J. Opt. Soc. Am. A **22**, 289–298 (2005).
26. J. Courtial and M. J. Padgett, "Limit to the orbital angular momentum per unit energy in a light beam that can be focussed onto a small particle," Opt. Commun. **173**, 269–274 (2000).
27. J. Arlt, "Handedness and azimuthal energy flow of optical vortex beams," J. Mod. Opt. **50**, 1573–1580 (2003).